Single Protein Molecule Detection by Glass Nanopores

Wenhong Li,[†,§] Nicholas A. W. Bell,[†,§] Silvia Hernández-Ainsa,[†] Vivek V. Thacker,[†] Alana M. Thackray,[‡] Raymond Bujdoso,[‡] and Ulrich F. Keyser[†,*]

[†]Cavendish Laboratory, University of Cambridge, J.J. Thomson Avenue, Cambridge CB3 0HE, United Kingdom, and [‡]Department of Veterinary Medicine, University of Cambridge, Madingley Road, Cambridge CB3 0ES, United Kingdom. [§]These authors contributed equally.

ABSTRACT Nanopores can be used to detect and analyze single molecules in solution. We have used glass nanopores made by laser-assisted capillary-pulling, as a high-throughput and low cost method, to detect a range of label-free proteins: lysozyme, avidin, IgG, β-lactoglobulin, ovalbumin, bovine serum albumin (BSA), and β-galactosidase in solution. Furthermore, we show for the first time solid state nanopore measurements of mammalian prion protein, which in its abnormal form is associated with transmissible spongiform encephalopathies. Our approach provides a basis for protein characterization and the study of protein conformational diseases by nanopore detection.

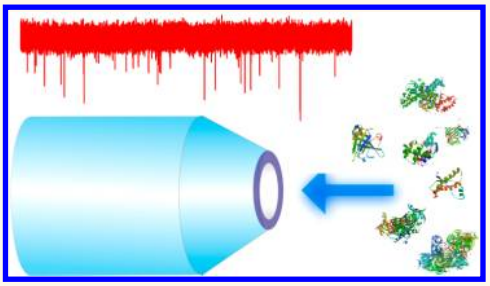

KEYWORDS: nanopores · nanocapillary · protein translocation · PrP · prions · single molecule detection · diagnosis

Nanopores are a promising technique for single molecule detection in solution. The premise of using nanopores for sensing is founded on the resistive-pulse technique,[1] which offers label-free detection and identification of single analytes in aqueous environments. The first application of resistive-pulse sensing for particle analysis was the Coulter Counter for detection of cells.[2] Subsequently, the technique has been expanded to include detection of particles such as pollen, viruses, or colloids coated with antibodies.[3−5] With a decreasing size of the detection pore, nanometer scale objects have been detected, such as organic polymers, peptides, proteins and DNA.[6,7]

Single protein molecules have been detected and their properties have been investigated using various types of nanopores. Biological nanopores, such as α-hemolysin or aerolysin, have been used collectively to detect small and unfolded proteins,[8−11] study the structure of peptides,[12] analyze peptide−antibody interactions,[13] and measure self−self peptide aggregation.[14] Biological nanopores have the advantage of a well-defined geometry but have a limitation in that the protein under analysis must be unfolded in order to translocate through the nanopore orifice, which is typically 1−2 nm in diameter. Solid state nanopores, which are more stable than biological nanopores, have also been used for the detection and analysis of single protein molecules.[14−19] Nanopores in a silicon nitride membrane have been used to enable detection of bovine serum albumin,[15,16] the folding states of β-lactoglobulin,[17] and to study protein−protein interactions.[18] With a PET membrane coated with gold nanotubes, one can distinguish BSA, phosphorylase B, and β-galactosidase by amplitude-duration scatter plots.[19] A lipid layer coating on a solid state nanopore can slow down protein transportation and eliminate nonspecific binding to the nanopore.[20] Positioning of a binding site in the nanopore gives specificity to protein measurements and enables determination of binding kinetics.[21] Glass capillaries have emerged as an alternative to both biological and silicon-based nanopores. They can be produced with orifice diameters ranging from micrometers to nanometers, with the advantages of ease of manufacture and relatively low cost. Glass nanopores have been successfully used to detect different biological molecules such as λ-DNA.[22−25]

Here, we show the ability of glass nanopores to detect a range of proteins of different molecular masses, including lysozyme (14 kDa), avidin (66 kDa), bovine β-lactoglobulin (18 kDa), ovalbumin (42 kDa), BSA (66 kDa), rabbit immunoglobulin G (IgG) (150 kDa), and β-galactosidase (465 kDa). In addition, we show for

* Address correspondence to ufk20@ cam.ac.uk.

Received for review January 28, 2013 and accepted April 10, 2013.

Published online 10.1021/nn4004567

the first time solid state nanopore measurements of the mammalian prion protein, PrP, which in its abnormal form is associated with transmissible spongiform encephalopathies, such as scrapie in sheep, bovine spongiform encephalopathy (BSE) in cattle, and Creutzfeldt–Jacob disease (CJD) of humans. These diseases are characterized by the accumulation of PrP^{Sc} (scrapie PrP), an abnormal isomer of the host protein PrP^{C} (cellular PrP). Recent work has shown that wild-type and mutant PrP^{C} can be distinguished by analyzing current fluctuations in an α-hemolysin protein pore.[26] Our demonstration of the detection of PrP and other single protein molecules of different molecular masses by glass nanopores provides the basis for the development of this technology as a novel method for protein detection and for analysis of the conformational state of disease-specific proteins with importance for human and animal health.

RESULTS AND DISCUSSION

We produced glass nanopores by laser-assisted capillary pulling. The glass nanopores were produced with smaller diameters and thicker walls (see Materials and Methods), compared with our previously reported experiments, significantly increasing signal-to-noise (see Supporting Information, Figure S2).[22] Figure 1a shows a lateral view scanning electron microscopy (SEM) image of a typical glass nanopore used in the experiments reported here. The outer diameter at the tip of the taper was 65 nm. Figure 1b shows a typical current–voltage (I–V) curve of a glass nanopore in 1 M KCl, buffered at pH 8 with 1× TE (10 mM Tris-HCl, 1 mM EDTA). All of the nanopores used in this paper showed linear I–V curves and had a conductance value in the range of 6.0 to 22.2 nS. The reservoir containing the glass nanopore tip was electrically grounded and samples were always added to this grounded reservoir. In the absence of analyte, no ionic current change events were evident in the current trace. Upon addition of the analyte to the reservoir, spikes became apparent in the current trace, which reflect the passage of analyte through the nanopore.

High Signal-to-Noise Ratio of Glass Nanopores. To demonstrate the high signal-to-noise ratio of our glass nanopores, we first investigated the detection of linear double-stranded λ-DNA (48.5 kbp) in our system. Ionic current change events were observed upon application of +500 mV when λ-DNA was present in the nanopore reservoir. Different peaks were clearly observed when plotting the histogram of the current points from 1079 λ-DNA translocations events (Figure 1c). These peaks correspond to different λ-DNA folding states. The signal-to-noise was significantly improved compared to our previously reported experiments[22] with a baseline signal root-mean-square (RMS) of 2.4 pA at 10 kHz bandwidth.

Effect of Filter Frequency on Event Duration and Mean Amplitude. Previous reports have shown that a 10 kHz filter cutoff frequency only captures a fraction of

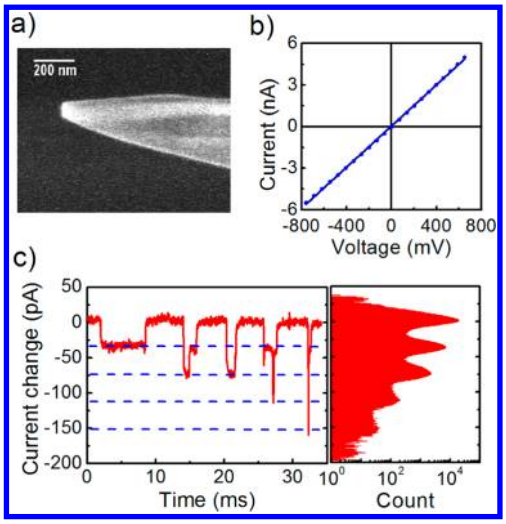

Figure 1. (a) SEM image shows the conical shape of a glass nanocapillary. The nanocapillary tapers down to form a glass nanopore at the tip. The outer diameter at the very tip of the nanocapillary was 65 nm. (b) I–V curve of one typical nanopore. A linear fit of these data (blue line) indicated a nanopore conductance of 6.8 nS. (c) Left: Typical ionic current change events. Right: Ionic current histogram of 1079 DNA translocation events that shows several peaks corresponding to DNA folding states. Data was recorded with a sampling frequency of 100 kHz and a filter cutoff frequency of 10 kHz.

protein translocation events due to the fast translocation dynamics.[27,28] Consequently, we examined the effect of the filter cutoff frequency on translocations of BSA through a glass nanopore at +500 mV applied potential in 1 M KCl, 1× TE (pH 8) (Figure 2a) at a sampling frequency of 500 kHz. The low noise of our glass nanopores allowed us to use filter cutoff frequencies at up to 100 kHz (the maximum filter frequency of the Axopatch 200B), and still have sufficient signal-to-noise ratio to detect individual protein translocation. We set a value of 8 times the RMS of the baseline signal as a threshold for event detection (see Supporting Information, Figure S3 for typical translocation events). Analysis of the translocation durations at different cutoff frequencies shows that the peak in duration shifts to shorter times at higher frequencies as we are able to capture more of the events as shown in Figure 2b. At the same time, the mean amplitude of the protein translocation events increased as the filter attenuation was reduced. Since the peak in the histogram moved to a shorter duration as the filter frequency was increased (and did not reach a fixed point despite an increase in filter frequency), we can conclude that at frequencies lower than 100 kHz we do not capture all the translocation events.

Detection of Single Protein Molecules. After the initial experiments with BSA already described, we investigated the ability of the glass nanopores to detect a range of proteins to determine their translocation characteristics. Figure 3 shows ionic current traces of the protein translocation experiments, which were

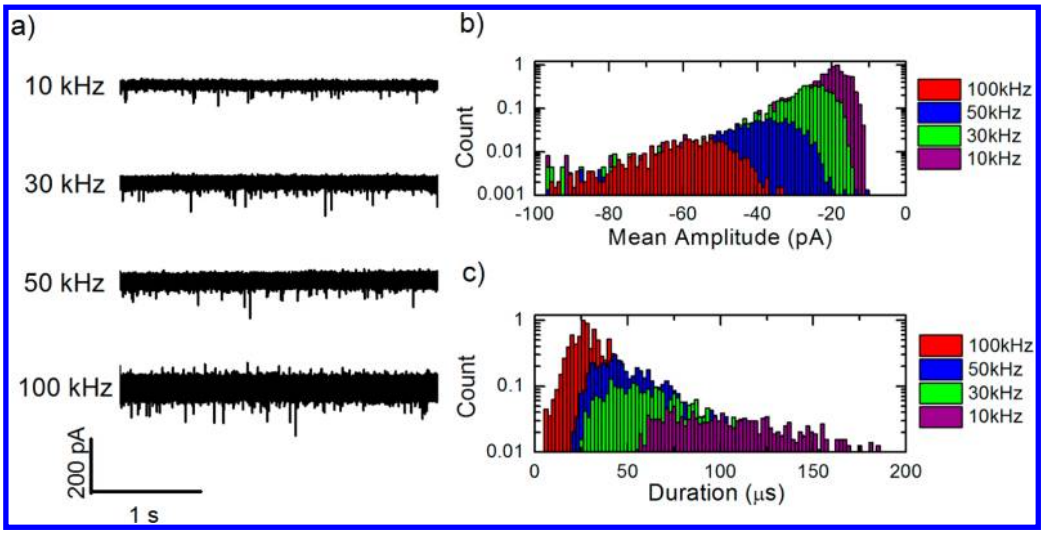

Figure 2. a) Current traces showing BSA translocation at different analog Bessel filter frequencies at +500 mV. b) The distributions of the mean amplitudes at different filter frequencies. The peak value of the 10 kHz distribution is normalized to 1. The peak value of the other histograms is normalized to the value of the 10 kHz distribution. c) The distributions of event duration at different filter frequencies. Distributions are normalized in the same way as (b).

conducted in 1 M KCl, 1× TE (pH 8). Size measurement of the proteins *via* dynamic light scattering (Malvern Zetasizer Nano ZS) showed that these salt conditions do not promote protein aggregation (see Supporting Information, Figure S4). After addition of protein to the nanopore reservoir, a positive or negative voltage (±500 mV) was applied and translocation events were sampled at 500 kHz. A 10 kHz Bessel filter was used for the detection of β-galactosidase and lysozyme since we could not obtain sufficient signal-to-noise with these proteins at higher filter frequencies. For all other proteins, a 50 kHz Bessel filter frequency was used. On the basis of our analysis in Figure 2, we expect that many of these events are distorted by the low pass filter cut off.

The isoelectric points (pI), concentrations and event frequencies for the proteins are shown in Table 1.

Protein translocations through nanopores are governed by the competing effects of electrophoresis and electro-osmosis.[29] At pH 8, the quartz surface of the glass nanopore is negatively charged.[30] Therefore, there will be an electro-osmotic flow from the electrically grounded reservoir into the glass nanopore when a negative voltage is applied and an oppositely directed flow when a positive potential is applied.

Avidin and lysozyme are both positively charged at pH 8 and we only observed translocations when a negative potential was applied across the system. Ovalbumin, BSA, β-lactoglobulin, and β-galactosidase are all negatively charged at pH 8 and were found to only translocate under positive potential. In the case of IgG, translocation events were observed when either a positive or negative voltage was applied across the system. This may have occurred as a result of the presence of different mixture subclasses of IgG in the immunoglobulin sample, each with different isoelectric

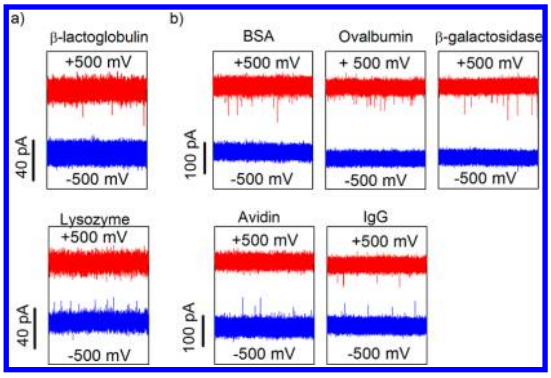

Figure 3. Current traces after the addition of proteins to the reservoir at positive (red line) and negative (blue line) applied voltage. Translocation spikes were only observed after addition of the protein to the analyte reservoir and the dependence of translocation on the polarity of the voltage correlates with the charge of the protein in solution. (a) A 10 kHz Bessel filter was used and the sampling rate was 100 kHz. (b) A 50 kHz Bessel filter was used at 500 kHz sampling rate. The time duration for each frame is 1 s.

points close to, or around, pH 8.[31] These experiments show that the direction of protein transport correlates with its charge at pH 8 and that electrophoretic transport dominates over electro-osmosis.

Figure 4 shows two dimensional scatter plots of mean amplitude *versus* event duration for each protein. All of the proteins show a cluster of events at the event duration limit imposed by the filter frequency. Outliers with long event durations are observable in most of the scatter plots. We hypothesize that these events are caused by transient adherence of the proteins as they translocate, whereas the main event clusters are due to proteins traveling ballistically through the nanopore. A simple model representing the glass nanopore as a cone and the protein as an insulating sphere predicts a strong dependence of current

TABLE 1. Isoelectric Points of Proteins Detected with Glass Nanopores[a], Concentration for Translocation Experiment, and the Average Translocation Frequency

	lysozyme	avidin	IgG[31]		β-lactoglobulin[17]	ovalbumin	BSA	β-galactosidase
pI	11	10	6–9		5	5	5	5
Concentration for translocation experiment	0.2 μM	1.5 μM	0.2 μM		0.6 μM	1.0 μM	0.6 μM	0.2 μM
Frequency of translocation events	104 s^{-1}	110 s^{-1}	+ 194 s^{-1}	- 518 s^{-1}	11 s^{-1}	111 s^{-1}	69 s^{-1}	131 s^{-1}

[a] Unreferenced values are from manufacturer's (Sigma Aldrich) Web site.

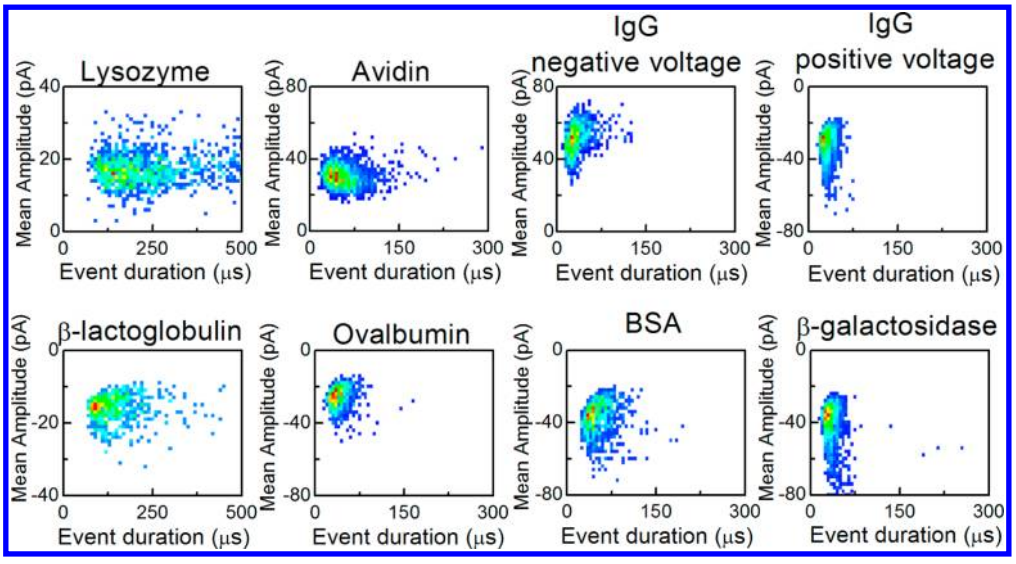

Figure 4. Two dimensional scatter plots of mean amplitude *versus* event duration of protein translocation experiments at 1 M KCl, 1× TE (pH 8). The frequency of events is indicated by the color scale. A 10 kHz filter was used in the lysozyme and β-lactoglobulin experiments which were recorded at 100 kHz sampling rate. A 50 kHz filter was used for the other proteins and recording performed at 500 kHz. Number of events: Lysozyme (1257), Avidin (3966), IgG positive voltage (7879), IgG negative (1330), β-lactoglobulin (1059), Ovalbumin (1820), BSA (2058), β-galactosidase (2551).

change on sphere radius (see Supporting Information, Figures S12–S14). Several factors can explain why we do not observe this in our scatter plots. (1) The proteins have different charges and hydrodynamic drags and will therefore move at different speeds through the nanopore. This will result in different levels of filter attenuation and distorted current changes. (2) Each protein is modeled as a completely insulating sphere in an excluded volume argument, whereas in reality, they will have a finite dielectric constant and also some permeability to ions. (3) Different proteins will have different tendencies to adhere to the sides of the walls as they translocate. It is very difficult to establish if translocations are completely ballistic or involve a transient adherence. This can also vary due to differences in the surface properties of different nanopores. We believe that a combination of these reasons make it extremely difficult to separate translocation signals of mixtures of proteins in these experiments. It should also be noted that different nanopores were used for each time frame in Figure 3; therefore, the small differences in nanopore geometry can affect the current change value. We also conducted experiments with mixtures in one single nanopore (see Supporting Information,

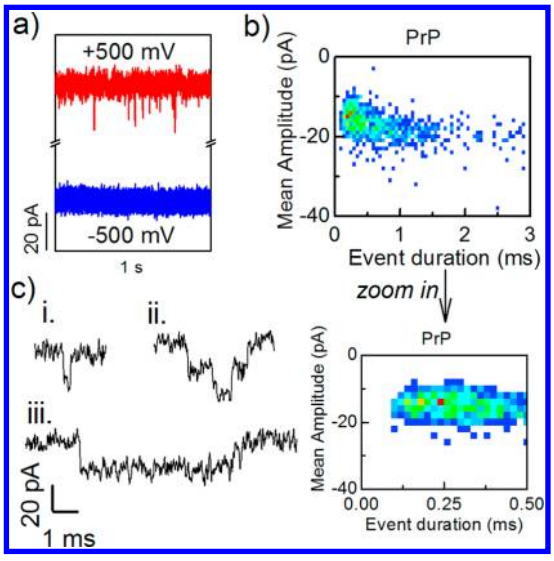

Figure 5. (a) Current trace showing PrP translocations in 1 M KCl, 1× TE (pH 8) upon applying positive voltage (red). No translocations are observed under negative voltage (blue). (b) Scatter plot of mean amplitude *versus* event duration of PrP translocation from a total of 952 events. (c) Three typical PrP events showing (i) fast translocation and (ii and iii) transient adherence.

TABLE 2. Parameters for Pipette Puller, for Figure 1 and Figure 5 in the Main Text

heat	filament	velocity	delay	pulling power
580	0	25	170	200

TABLE 3. Parameters for Pipette Puller, for Figures 2–4 in the Main Text

heat	filament	velocity	delay	pulling power
600	0	25	170	225

Figures S9–S11) but were not able to discern clear differences in protein translocation signals.

Detection of PrP. After the successful detection of a range of commonly available proteins, we investigated the ability of our nanopore system to detect PrP, the protein associated with prion diseases in humans and animals. PrP translocations were detected in a solution of 1 M KCl, 1× TE (pH 8). Current data was filtered at 20 kHz and recorded at 200 kHz sampling rate. We observed translocation events under positive voltage but not under negative voltage (Figure 5a). This indicates that the protein is negatively charged at pH 8. The event scatter plot is qualitatively similar to the previously measured proteins with a cluster of events close to the limit imposed by the filter and a tail of longer duration events (Figure 5b). Figure 5c shows three typical current traces for PrP. Event (i) is of short duration, suggesting ballistic transport. Event (ii) is several milliseconds in duration and has two levels, suggesting transient adherence of two PrP molecules to the sides of the nanopore walls. Event (iii) shows a longer duration sticking event.

CONCLUSION

We demonstrate single molecule detection of a range of proteins. These experiments extend the range of ionic current detection of glass nanopores, which are simple and inexpensive alternatives to those formed by ion or electron beam drilling in silicon nitride membranes. The translocation direction of the protein correlates with its overall charge in solution and allows for characterization of mixtures of proteins, such as IgG. Furthermore, we show the first solid state nanopore measurements of mammalian prion protein PrP that provide a basis to study protein misfolding and aggregation at the nanoscale level.

METHODS AND MATERIALS

Protein Preparation. Proteins used in Figures 2–4 were dissolved in 0.2 μm filtered deionized water, stored at 4 °C, and used within two days of preparation. PrP was stored at −80 °C before use and in 50 mM sodium acetate (pH 5.5). The concentration of proteins used in the translocation experiments is shown in Table 1. A different concentration of each protein was used in these experiments in order to maximize the frequency of translocation events.

Production of Glass Nanopores. Glass nanopores were prepared by laser-assisted capillary-pulling of quartz glass capillaries. For this purpose, we used glass capillaries that possessed a filament, which greatly improved wetting and reduced the number of capillaries obstructed with air bubbles. Before pulling, quartz glass capillaries with an outer diameter of 0.5 mm and an inner diameter of 0.2 mm were thoroughly cleaned by sonication in acetone and subsequently dried with gaseous nitrogen. Glass nanopores were formed by laser assisted pulling of the capillaries (Sutter P-2000). Two glass nanopores were formed as the capillary shrank in diameter and finally separated at its center. Table 2 shows the specific parameters of the pipet puller used to generate glass nanopores for the detection of DNA and PrP (data shown in Figure 1 and Figure 5, respectively). Table 3 shows the specific parameters of the glass puller used to generate glass nanopores for the analysis of lysozyme, avidin; β-lactoglobulin, ovalbumin, BSA; IgG and β-galactosidase data (data shown in Figures 2–4).

SEM Preparation. Uncoated glass nanopores were imaged with a Philips XL30 FEGSEM. The acceleration voltage was 2 kV.

Assembly of Measurement Cells. The glass nanocapillary was inserted in a polydimethylsiloxane (PDMS) mold and sealed so that it was the sole electrical connection between two reservoirs. The assembled devices were plasma cleaned for 10 min to remove any organic contaminants as well as to enhance the wettability of the nanopores. Immediately after the plasma treatment, the two reservoirs were filled with 1 M KCl, 1× TE (pH 8) and placed in a vacuum for approximately 5 min in order to remove all air inside the capillaries. Ionic currents were recorded with Ag/AgCl electrodes made by electroplating.

Data Acquisition. All ionic current measurements were made using an Axopatch 200B (Axon Instruments, USA) amplifier in voltage-clamp mode. The signals were digitized with a NI-PCIe-6251 card (National Instruments). Data recording and analysis were performed with a custom program written in LabVIEW (LabVIEW 8.6, National Instruments).

Recombinant PrP Preparation. Recombinant PrP was purified from BL21(DE3)pLysS *Escherichia coli* that expressed mature length VRQ ovine prion protein (amino acids 25–232) using a method adapted from Hornemann *et al.*[32] and described in detail previously.[33] Oxidized and refolded recombinant PrP was stored at −80 °C.

Conflict of Interest: The authors declare no competing financial interest.

Acknowledgment. W.L., S.H.-A. and U.F.K. acknowledge support from an ERC starting grant. N.A.W.B. was supported by a studentship from the EPSRC NanoDTC program. V.V.T. is grateful to the Cambridge Commonwealth Trust, the Jawaharlal Nehru Memorial Trust, and the Emmy Noether program for the Deutsche Forschungsgemeinschaft for support of his Ph.D. position.

Supporting Information Available: Schematic graph of system, noise reduction by using thick walled capillaries, typical protein translocation events, hydrodynamic diameter of proteins, voltage effects on mean current amplitude, noise event analysis, data analysis algorithm, reproducibility of protein translocation data, detection of mixtures of proteins, resistive pulse modeling of protein translocation. This material is available free of charge *via* the Internet at http://pubs.acs.org.

REFERENCES AND NOTES

1. Bayley, H.; Martin, C. R. Resistive-Pulse Sensing: from Microbes to Molecules. *Chem. Rev.* **2000**, *100*, 2575–2594.
2. Kubitschek, H. E. Electronic Counting and Sizing of Bacteria. *Nature* **1958**, *182*, 234–235.

3. Zhang, Z.; Zhe, J.; Chandra, S.; Hu, J. An Electronic Pollen Detection Method Using Coulter Counting Principle. *Atmos. Environ.* **2005**, *39*, 5446–5453.
4. DeBlois, R. W.; Wesley, R. K. Sizes and Concentrations of Several Type C Oncornaviruses and Bacteriophage T2 by the Resistive-Pulse Technique. *J. Virol.* **1977**, *23*, 227–233.
5. Carbonaro, A.; Sohn, L. L. A Resistive-Pulse Sensor Chip for Multianalyte Immunoassays. *Lab. Chip* **2005**, *5*, 1155–1160.
6. Majd, S.; Yusko, E. C.; Billeh, Y. N.; Macrae, M. X.; Yang, J.; Mayer, M. Applications of Biological Pores in Nanomedicine, Sensing, and Nanoelectronics. *Curr. Opin. Biotechnol.* **2010**, *21*, 439–476.
7. Bell, N. A. W.; Engst, C. R.; Ablay, M.; Divitini, G.; Ducati, C.; Liedl, T.; Keyser, U. F. DNA Origami Nanopores. *Nano Lett.* **2011**, *12*, 512–517.
8. Stefureac, R.; Waldner, L.; Howard, P.; Lee, J. S. Nanopore Analysis of a Small 86-Residue Protein. *Small* **2008**, *4*, 59–63.
9. Oukhaled, G.; Mathé, J.; Biance, A. L.; Bacri, L.; Betton, J. M.; Lairez, D.; Pelta, J.; Auvray, L. Unfolding of Proteins and Long Transient Conformations Detected by Single Nanopore Recording. *Phys. Rev. Lett.* **2007**, *98*, 158101.
10. Pastoriza-Gallego, M.; Rabah, L.; Gibrat, G.; Thiebot, B.; van der Goot, F. G.; Auvray, L.; Betton, J.-M.; Pelta, J. Dynamics of Unfolded Protein Transport Through an Aerolysin Pore. *J. Am. Chem. Soc.* **2011**, *133*, 2923–2931.
11. Stefureac, R.; Long, Y.-t.; Kraatz, H.-B.; Howard, P.; Lee, J. S. Transport of α-Helical Peptides through α-Hemolysin and Aerolysin Pores. *Biochemistry* **2006**, *45*, 9172–9179.
12. Sutherland, T. C.; Long, Y.-T.; Stefureac, R.-I.; Bediako-Amoa, I.; Kraatz, H.-B.; Lee, J. S. Structure of Peptides Investigated by Nanopore Analysis. *Nano Lett.* **2004**, *4*, 1273–1277.
13. Madampage, C. A.; Andrievskaia, O.; Lee, J. S. Nanopore Detection of Antibody Prion Interactions. *Anal. Biochem.* **2010**, *396*, 36–41.
14. Wang, H.-Y.; Ying, Y.-L.; Li, Y.; Kraatz, H.-B.; Long, Y.-T. Nanopore Analysis of β-Amyloid Peptide Aggregation Transition Induced by Small Molecules. *Anal. Chem.* **2011**, *83*, 1746–1752.
15. Han, A.; Schurmann, G.; Mondin, G.; Bitterli, R. A.; Hegelbach, N. G.; de Rooij, N. F.; Staufer, U. Sensing Protein Molecules Using Nanofabricated Pores. *Appl. Phys. Lett.* **2006**, *88*, 093901.
16. Fologea, D.; Ledden, B.; McNabb, D. S.; Li, J. Electrical Characterization of Protein Molecules by a Solid-State Nanopore. *Appl. Phys. Lett.* **2007**, *91*, 053901.
17. Talaga, D. S.; Li, J. Single-Molecule Protein Unfolding in Solid State Nanopores. *J. Am. Chem. Soc.* **2009**, *131*, 9287–9297.
18. Han, A.; Creus, M.; Schürmann, G.; Linder, V.; Ward, T. R.; de Rooij, N. F.; Staufer, U. Label-Free Detection of Single Protein Molecules and Protein−Protein Interactions Using Synthetic Nanopores. *Anal. Chem.* **2008**, *80*, 4651–4658.
19. Sexton, L. T.; Mukaibo, H.; Katira, P.; Hess, H.; Sherrill, S. A.; Horne, L. P.; Martin, C. R. An Adsorption-Based Model for Pulse Duration in Resistive-Pulse Protein Sensing. *J. Am. Chem. Soc.* **2010**, *132*, 6755–6763.
20. Yusko, E. C.; Johnson, J. M.; Majd, S.; Prangkio, P.; Rollings, R. C.; Li, J.; Yang, J.; Mayer, M. Controlling Protein Translocation through Nanopores with Bio-Inspired Fluid Walls. *Nat. Nano* **2011**, *6*, 253–260.
21. Wei, R.; Gatterdam, V.; Wieneke, R.; Tampe, R.; Rant, U. Stochastic Sensing of Proteins with Receptor-Modified Solid-State Nanopores. *Nat. Nano* **2012**, *7*, 257–263.
22. Steinbock, L. J.; Otto, O.; Chimerel, C.; Gornall, J.; Keyser, U. F. Detecting DNA Folding with Nanocapillaries. *Nano Lett.* **2010**, *10*, 2493–2497.
23. Hernández-Ainsa, S.; Muus, C.; Bell, N. A. W.; Steinbock, L. J.; Thacker, V. V.; Keyser, U. F. Lipid-Coated Nanocapillaries for DNA Sensing. *Analyst* **2013**, *138*, 104–106.
24. Thacker, V. V.; Ghosal, S.; Hernández-Ainsa, S.; Bell, N. A. W.; Keyser, U. F. Studying DNA Translocation in Nanocapillaries Using Single Molecule Fluorescence. *Appl. Phys. Lett.* **2012**, *101*, 223704.
25. Steinbock, L. J.; Otto, O.; Skarstam, D. R.; Jahn, S.; Chimerel, C.; Gornall, J. L.; Keyser, U. F. Probing DNA with Micro- and Nanocapillaries and Optical Tweezers. *J. Phys.: Condens. Matter* **2010**, *22*, 454113.
26. Jetha, N. N.; Semenchenko, V.; Wishart, D. S.; Cashman, N. R.; Marziali, A. Nanopore Analysis of Wild-Type and Mutant Prion Protein (PrP^C): Single Molecule Discrimination and PrP^C Kinetics. *PLoS One* **2013**, *8*, e54982.
27. Pedone, D.; Firnkes, M.; Rant, U. Data Analysis of Translocation Events in Nanopore Experiments. *Anal. Chem.* **2009**, *81*, 9689–9694.
28. Plesa, C.; Kowalczyk, S. W.; Zinsmeester, R.; Grosberg, A. Y.; Rabin, Y.; Dekker, C. Fast Translocation of Proteins through Solid State Nanopores. *Nano Lett.* **2013**, *13*, 658–663.
29. Firnkes, M.; Pedone, D.; Knezevic, J.; Döblinger, M.; Rant, U. Electrically Facilitated Translocations of Proteins through Silicon Nitride Nanopores: Conjoint and Competitive Action of Diffusion, Electrophoresis, and Electroosmosis. *Nano Lett.* **2010**, *10*, 2162–2167.
30. Umehara, S.; Pourmand, N.; Webb, C. D.; Davis, R. W.; Yasuda, K.; Karhanek, M. Current Rectification with Poly-l-Lysine-Coated Quartz Nanopipettes. *Nano Lett.* **2006**, *6*, 2486–2492.
31. Loeken, M. R.; Roth, T. F. Analysis of Maternal IgG Subpopulations which are Transported into the Chicken Oocyte. *Immunology* **1983**, *49*, 21–28.
32. Hornemann, S.; Korth, C.; Oesch, B.; Riek, R.; Wider, G.; Wüthrich, K.; Glockshuber, R. Recombinant Full-Length Murine Prion Protein, mPrP(23−231): Purification and Spectroscopic Characterization. *FEBS Lett.* **1997**, *413*, 277–281.
33. Wong, E.; Thackray, A. M.; Bujdoso, R. Copper Induces Increased Beta-Sheet Content in the Scrapie-Susceptible Ovine Prion Protein PrPVRQ Compared with the Resistant Allelic Variant PrPARR. *Biochem. J.* **2004**, *380*, 273–282.